Role of the lower hybrid spectrum in the current drive modeling for DEMO scenarios

Role of the lower hybrid spectrum in the current drive modeling for DEMO scenarios

A Cardinali[1], C Castaldo[1], R Cesario[1], F Santini[1], L Amicucci[2], S Ceccuzzi[1], A Galli[2], F Mirizzi[3], F Napoli[1], L Panaccione[3], G Schettini[4] and A A Tuccillo[1]

[1] ENEA, Fusion and Nuclear Safety Department, C. R. Frascati, Via E. Fermi 45, I-00044 Frascati (Rome), Italy
[2] Università Roma La Sapienza, Dipartimento di Ingegneria, Rome, Italy
[3] CREATE, Via Claudio 21, I-80125, Napoli, Italy
[4] Università Roma Tre, Dipartimento di Ingegneria, Rome, Italy

E-mail: alessandro.cardinali@enea.it

CrossMark

Abstract

The active control of the radial current density profile is one of the major issues of thermonuclear fusion energy research based on magnetic confinement. The lower hybrid current drive could in principle be used as an efficient tool. However, previous understanding considered the electron temperature envisaged in a reactor at the plasma periphery too large to allow penetration of the coupled radio frequency (RF) power due to strong Landau damping. In this work, we present new numerical results based on quasilinear theory, showing that the injection of power spectra with different $n_{//}$ widths of the main lobe produce an RF-driven current density profile spanning most of the outer radial half of the plasma ($n_{//}$ is the refractive index in a parallel direction to the confinement magnetic field). Plasma kinetic profiles envisaged for the DEMO reactor are used as references. We demonstrate the robustness of the modeling results concerning the key role of the spectral width in determining the lower hybrid-driven current density profile. Scans of plasma parameters are extensively carried out with the aim of excluding the possibility that any artefact of the utilised numerical modeling would produce any novelty. We neglect here the parasitic effect of spectral broadening produced by linear scattering due to plasma density fluctuations, which mainly occurs for low magnetic field devices. This effect will be analyzed in other work that completes the report on the present breakthrough.

Keywords: lower hybrid, current drive, ITER, DEMO, tokamak reactor

(Some figures may appear in colour only in the online journal)

1. Introduction

Reactor-oriented devices such as ITER [1, 2] (now in construction phase), ARIES [3] and DEMO [4–6] will demonstrate the scientific and technological feasibility of fusion energy power stations. In particular, DEMO encompasses two main projects: a steady state reactor which is considered today as a second option due to the difficulty of driving non-inductive current, and a pulsed reactor where the main current is still inductive. In the latter, the thermonuclear plasma would exploit the high (H-) confinement mode that is formed when strong heating power is injected, and is characterized by a steep profile with high pressure even at the edge of the plasma column, where the so-called pedestal is formed [7]. In order to provide fusion performance, the condition of high values of electron density ($n_e \approx 7 \times 10^{19}$ m^{-3}) and temperature ($T_e \approx 8$ keV) of plasma electrons should be sustained, at least for several hours, at the pedestal radial layer (at the normalized minor radius, $x \equiv r/a \approx 0.9$, where a corresponds to the last closed magnetic surface). This current flat-top phase is obtained after a current ramp-up

phase, in which strong heating and current drive (CD) are suitably performed by neutral beam and radio frequency (RF) power. To guarantee the energy gain produced by fusion reactions occurring during this phase, it is necessary to utilize the large fraction of non-inductive plasma current self-produced by particle transport mechanism via the pressure-gradient-driven bootstrap effect [5, 7]. This current fraction (j_{BS}) which naturally develops, especially in the outer half radius (the pedestal layer), favours the achievement of the necessary conditions of thermal insulation and stability in a large plasma volume [7]. Nevertheless, these conditions can not necessarily persist as required since j_{BS} intrinsically depends upon (also minor) changes to local pressure shapes that occur unpredictably during operations. A reactor should thus be provided with a system of current profile control, but this is problematic since an efficient CD tool capable of actively covering the critical region that the outer radial half of plasma column represents is not available so far. This problem could seriously jeopardize the progress of pulsed reactor research. Therefore, an efficient RF system to drive plasma current is necessary in a steady state as well as in a pulsed reactor project. This task could be performed by coupling strong RF power to lower hybrid (LH) waves via waveguide antennas, which allows the production of the lower hybrid current drive (LHCD) effect (in principle, the most efficient method available so far for driving current in tokamak plasmas [8]). The fact that the electron temperature at the reactor pedestal is too high could inhibit efficient penetration of the coupled RF power due to strong Landau damping, and could frustrate the current profile control over the desirable radial domain. Moreover, due to the accessibility condition, the high density of a thermonuclear plasma requires launched antenna spectra with $n_{//}$ greater than in the present machines, which would undesirably enhance Landau damping and favour more peripheral RF power deposition ($n_{//}$ is the refractive index in direction parallel to the confinement magnetic field). The present study, based on the WKB description of wave propagation in the framework of standard quasilinear (QL) theory, shows that RF power deposition can be usefully tailored by changing the antenna power spectrum. The latter is numerically modelled by a tool able to treat antenna structures, however complex [9]. An $n_{//}$ antenna spectrum with a sufficiently narrow main lobe at the minimum accessible $n_{//}$ moderates the strong absorption expected in a high-temperature plasma and allows the wave packet to reach inner layers. Passive active multijunction (PAM) antennas realistically designed for ITER and DEMO have been considered in this analysis [10]. The $n_{//}$ peak and width of the main lobe of the antenna can be set by appropriately feeding and phasing the waveguides in order to get fine control of the RF power and the driven current density radial profiles. The mechanism of linear scattering by plasma density fluctuations [11] that indeed broadens the launched antenna spectrum in the presence of a magnetic field of confinement which is too low is described in [12]. The latter reference, consequently, displays the conditions for real exploitability of the present breakthrough in reactor plasmas. [12] also displays a detailed analytical modeling, based on standard QL theory, which

shows the role of the $n_{//}$ width in determining the absorption of the wave packet in the plasma, consistently with results obtained by the numerical tool utilised here.

The paper is organized as follows. In section 2, the role of the LH wave as a tool for sustaining current drive in tokamak reactor is highlighted. In section 3, the main features of the numerical calculations and the integrated numerical tools used for this analysis are described. In section 4, the numerical results for DEMO I are presented and discussed. Section 5 is devoted to a very accurate study of the sensibility of the numerical model as a function of the main plasma and antenna parameters. Finally, in section 6 conclusive remarks are presented.

2. The role of the LH wave

The lower hybrid current drive (LHCD) [8, 13, 14] was recognized as attractive for a reactor since non-inductive current is efficiently produced in a plasma by LH waves launched by a phased array of waveguide antennas. Such structures fit the very large ports through the tokamak reactor magnet gaps and are capable of coupling strong RF power of several gigahertz. These waves are absorbed by electron Landau damping at the limit where the quasi-linear (QL) approximation [15–20] holds. This involves a velocity tail of the electron distribution function (EDF) [21]:

$$u_{\phi//} \approx \frac{\omega_0}{k_{//}} = \frac{c}{n_{//}} \geqslant 3\, u_{the} \tag{1}$$

where $u_{\phi//}$ is the wave phase velocity, the suffix '//' refers to the direction parallel to the equilibrium magnetic field, ω_0 is the operating angular frequency, $k_{//}$ is the wave-vector parallel component, c is the light speed, $n_{//} = ck_{//}/\omega_0$ is the parallel refractive index component, $u_{the} = \sqrt{\kappa T_e/m_e}$ is the electron thermal velocity and the other quantities have the usual meaning.

In order to model LH wave propagation in the plasma, the ray trajectory model is used in the geometric optic approximation, referred to as WKB limit to describe the relevant propagation problems [22, 23]. However, this approximation fails in the regions of plasma edge where the cut-offs of LH wave are located, since too large wavelength locally occurs. This problem does not however interest a reactor, which is intrinsically free from multi-radial reflections from the walls of the machine, owing to strong Landau damping occurring in hot plasma. This produces indeed full deposition of the launched RF power at the first half radial pass of the launched RF power.

Two major problems have prevented for a long time the extrapolation of the LHCD method to the reactor relevant conditions, namely the high values of plasma density and temperature.

The problem of high density concerns the excitation of parametric instability (PI) occurring at the plasma edge and at the radial periphery in standard operating conditions of high plasma densities in tokamak experiments performed so far [24–28]. The problem of the PI effect was investigated and

solved by a new method established on Frascati Tokamak Upgrade (FTU) under operation of higher temperature of plasma edge and periphery, as previously predicted by theory [29]. The latter result suggests that PI would not produce significant effects in high-temperature conditions envisaged in the reactor, even at the plasma edge. For the considered kinetic profiles of DEMO plasma, PI analysis, reported further on in the paper, shows that the plasma is stable at radii inner or close to the last closed magnetic surface (LCMS), thanks to the occurring large T_e values (>0.5 keV). Similarly, the much colder (with $T_e \approx 10$ eV) scrape-off layer (SOL), as that envisaged for ITER [1], produces PI suppression by collision effect [30] and by convective loss due to plasma inhomogeneity which maximises at radii closer to LCMS [30, 31].

The remaining problem thus consists of the excessively strong Landau damping consequence of high T_e values envisaged for DEMO even at the pedestal layer [4, 32]. The useful width of the $n_{//}$ spectrum is bounded to the lower values by the LH wave accessibility condition, which is necessary for avoiding the mode-conversion of LH waves into fast waves. This occurs for excessively high-value plasma density and excessively low toroidal magnetic field (B_T) [22]. At the higher $n_{//}$ values of the spectrum, electron damping takes place at larger radii as the waves meet regions where T_e is increasing and the EDF tail of (1) develops rapidly. Thus the residual part of the spectrum that is useful for QL absorption inside the plasma is believed to be a small fraction of the full launched spectrum, even if the effects of spectral broadening are not present, as assumed in the present analysis. A feedback-like mechanism, based on the mutual QL interaction of the single spectral components, determines the full wave absorption and the LHCD effect in the plasma [12, 33]. As the wave penetrates towards the hot core, the development of the EDF tail due to the higher $n_{//}$ (lower velocities) of the spectrum promotes the absorption of spectral components with smaller and smaller $n_{//}$ values. This feedback-like mechanism, based on the mutual QL interaction of the single spectral components, determines the full wave absorption and the LHCD effect in the plasma. Therefore, a larger spectrum is absorbed rapidly at the plasma periphery. On the contrary, for a given T_e profile, an antenna power spectrum with a proper central $n_{//0}$ and a relatively small width of the main lobe ($\Delta n_{//}$ is kept at half of the power peak) would be, in principle, capable of activating the QL interaction at more internal radii, as desirable for a reactor [12, 33]. To assess this effect under different conditions of density and temperature envisaged in rector plasma represents the main focus of this paper. Wave absorption takes place, however, in a single half radial pass, and the numerical code described hereafter is fully appropriate for this reactor-relevant condition. The wave ray path towards the plasma core is short and similar to the original 'resonant cone' of LH theory. Here, a relatively high RF power density favours a somewhat smaller QL absorption rate, thus inner wave penetration. The large dimensions of the reactor accesses allow not only the coupling of RF power high enough to drive a sizable plasma current, but also the insertion of a grill array of many waveguides capable of coupling very narrow spectra in the frequency range of 5 GHz.

3. Numerical modeling

For the numerical analysis of LH propagation and absorption in tokamak reactor plasma parameters range, the LH^{star} package has been used, which consists of the following suite of numerical codes: (i) the Grill-3D module [9], (ii) the lower hybrid parametric instability (LHPI) module [24, 25, 31], which computes the PI effect of broadening the antenna spectrum, and (iii) the RayFP module [34] that uses as input the spectrum provided by the LHPI tool, and models the j_{LH} profile via ray-tracing computation in toroidal geometry and Fokker–Planck analysis. (Some of the quoted references do not display the tool name, given more recently). The ray-tracing technique has, however, been used in conditions fulfilling the WKB limit, as routinely done in previous works utilizing this package, relevant to performed LHCD experiments mentioned hereafter. In particular Grill-3D produces, given the antenna design, a very accurate power spectrum at the plasma edge in the toroidal and poloidal components of the wavenumber as well as the antenna directivity. Not only this, but playing with the waveguide feeding and antenna dimensions it is also possible to change the shape and width of the power spectrum on the main peak. The power spectrum and the plasma edge parameters are used as input for the parametric instability analysis that leads to redefining the power spectrum really coupled to the plasma. The ray-tracing Fokker–Planck package solves the problem of wave penetration and absorption inside the plasma, keeping in account the real magnetic structure of the tokamak and using geometric optic approximation (ray tracing). Each component of the wave spectrum (N components) is followed by solving N coupled ray-tracing equations for the space, wavenumber and damping rate $\left(\frac{1}{P} \frac{dP}{dx} = -2k_{\perp}^{Im} \right)$ by iterating with the Fokker–Planck module on each magnetic surface, in which the plasma has been divided. The Fokker–Planck module produces the local electron distribution function and its first derivative in the velocity space. The quasi-linear damping rate, in fact, is proportional to the first derivative of the distribution function on the resonant velocity $v_{//} = \omega/k_{//}$, and is calculated self-consistently on the given magnetic surface. As a result, the local power deposition and the current driven profiles can be obtained. The calculation is repeated until all the power carried by the ray is exhausted. Once this calculation is concluded, all the LHCD-relevant quantities like the global absorbed power, generated current, efficiency etc can be evaluated.

The code robustness has been supported by considering the JET parameters in experiments devoted to sustain confinement and stability in advanced tokamak regimes [35–37]. LH modeling performed with the same approach adopted here showed that the coupled LH power was absorbed at the first half radial pass, like in a reactor. Moreover, the j_{LH} profile resulted in agreement with experimental CD data, and was
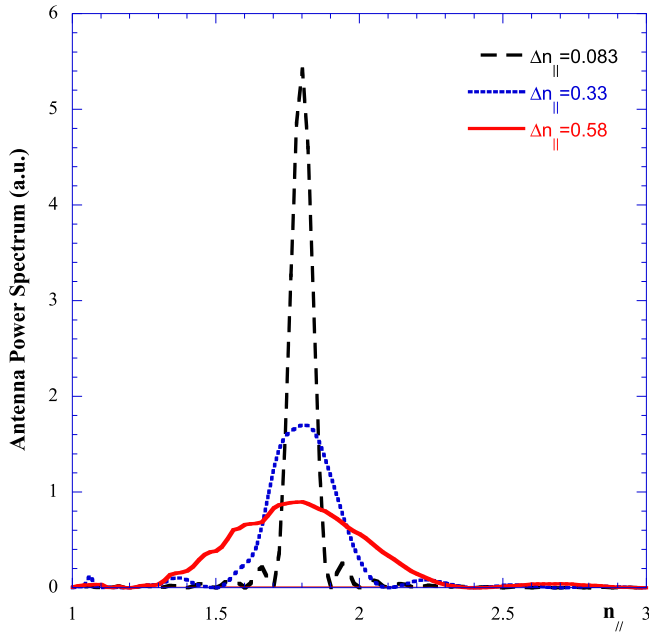
Figure 1. Main lobe of the antenna spectra obtained by a passive active multijunction (PAM) waveguide antenna, with modules phased for launching spectra with the same *n* // peak but with three different widths, respectively, $\Delta n_{//} = 0.083$ (black curve), $\Delta n_{//} = 0.33$ (blue curve) and $\Delta n_{//} = 0.58$ (red curve). Minor lobes occurring in the full spectral range are not displayed (see the text).

consistent with the plasma confinement improvement produced by LHCD within a certain radial layer (i.e. the so-called transport barrier radial foot) [24, 25]. The latter references contain also theoretical predictions which are useful for solving the LHCD in the high-plasma density regime that characterizes tokamak reactor design [29, 33]. In the latter work, consistency was found between modeling and experimental data.

4. LH penetration in reactor plasma

We show here new modeling results that, by taking advantage of the proper aspects of the complex wave physics governed by QL theory, are relevant to the problem of how to actively shape the current profile of reactor plasma. This goal is reached by a new key parameter, $\Delta n_{//}$ the width of the antenna spectrum, which can be set within a range wider than in present devices thanks to the larger size of reactor access ports. Previous works have generally kept $\Delta n_{//}$ as a fixed parameter [38, 39]. Instead here we let the spectrum width vary around narrow values while keeping the central $n_{//0} = 1.8$ (which is the most convenient value to favor inner absorption and to avoid accessibility problems) fixed.

Typical spectra are shown in figure 1. Here the main lobe of the three antenna power spectra having the same $n_{//0} = 1.8$ but different widths is shown. These figures, corresponding to different antenna phasing, are calculated using the Grill-3D numerical code [9], capable of considering very complicated geometries. Namely, the LHCD antenna considered here for DEMO [40] consists of the same modules

proposed for ITER [10], but larger dimensions of about 1.2 m in the toroidal direction and 2.2 m in the poloidal direction are assumed. A somewhat larger antenna-plasma interface is also considered.

A strong RF power coupled to the plasma is assumed ($P_{LH} = 80$ MW) at a frequency of 5 GHz. These conditions guarantee safe operations since they correspond to power density ($p_{RF} \approx 30$ MW m^{-2}) of about half of the limit ($p_{LH} = 60$ MW m^{-2}) expected from experiments at this frequency [41]. The antenna type is a passive active multi-junction (PAM) waveguide array [10], consisting of two piles of (38) rows, placed side by side, and suitably fed to launch the desired $n_{//0}$ and $\Delta n_{//}$ parameters. Each row (size 615.5 mm) is aligned to the toroidal direction, and consists of (24) active waveguides and (25) passive waveguides (i.e. the latter are not fed). The sizes of each waveguide are: width 9.5 mm, height 58 mm, wall thickness 3 mm, and phase shift between active waveguides 90°.

The spectra of figure 1 have been chosen to satisfy the LH wave accessibility condition for the considered dense plasma density profile; their different widths ($\Delta n_{//} = 0.083$, $\Delta n_{//} = 0.33$ and $\Delta n_{//} = 0.58$) have been considered for modeling the current drive effect. Currently, the whole antenna spectrum, corresponding to the above case of narrow main lobe, exhibits well-separated secondary peaks (at $n_{//} = -3.2$; -6; -8 and $n_{//} = +6.5$: positive/negative values correspond to LH waves travelling in the co-/counter direction of the plasma current). The resulting net CD takes into account the antenna directivity ($dir \equiv P_+/(P_+ + P_-)$, where P_+ and P_- indicate, respectively, the wave power fraction travelling in the co- and counter plasma current direction).

The DEMO parameters, shown for example in [4–6] and obtained self consistently by using 2D transport codes in a realistic magnetic configuration, have been considered for the present analysis (the major radius is $R = 9$ m and the minor plasma radius on the equatorial plane is $a = 2.25$ m, $B_T = 6.8$ T). Two configurations, respectively, with density profiles 'peaked' and 'flat', envisaged for the DEMO pulsed regime, have been considered. In the former case, the plasma current is $I_p = 22$ MA and in the latter case, $I_p = 18$ MA. The density and temperature radial profiles are shown in figure 2. The highest T_e value occurs for the 'flat' case of figure 2, which would produce, on the basis of present understanding, LHCD effect more at the plasma periphery as a consequence of the $T_{e-pedestal}$ being too high [5, 20]. Note that for both peaked and flat configuration of DEMO, the temperature at the pedestal (7–9 keV) is much higher than that of ITER (1–2 keV). For comparison, the figure also displays the respective profiles for the steady-state scenario envisaged for ITER [42, 43]. It is worth recalling here that simulations of LHCD for plasma parameters related to ITER scenario 4 and 2 have been performed in the past by several authors [42–45]. The results of these simulations with the antenna parameter calculated consistently by coupling codes are similar to that obtained by the present analysis. We want to stress here that the present analysis is related to the DEMO reactor whose plasma parameters are more critical for LH propagation and
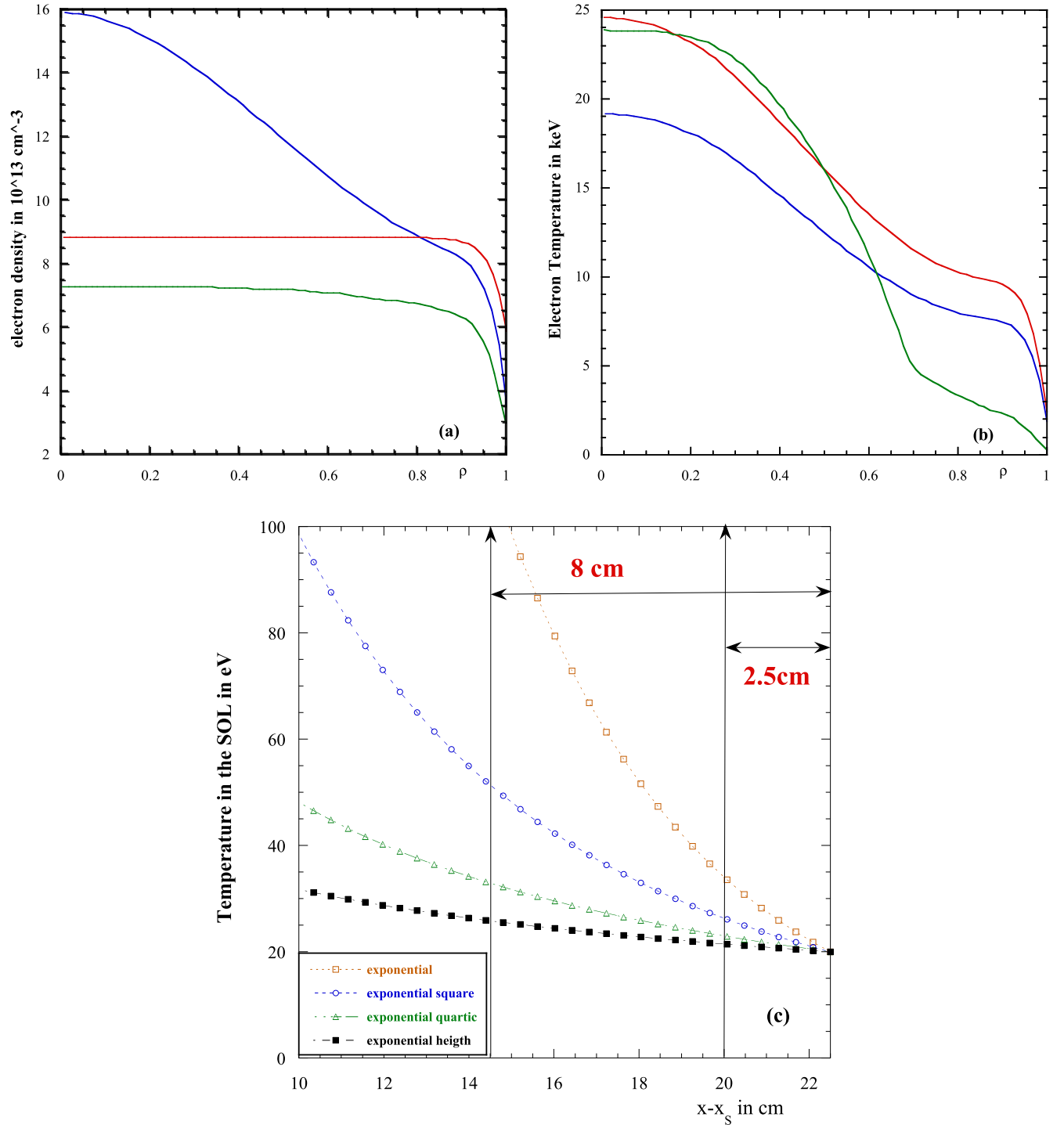
Figure 2. Electron plasma radial profiles of: (a) density and (b) temperature envisaged for the DEMO pulsed regime, with peaked (blue curves) and flat (red curves) scenarios. Steady-state regime profiles of ITER (green curves) are also displayed. (c) Shows the electron temperature SOL profiles used in PI analysis.

absorption than those in ITER, and the solutions found here in controlling the power deposition layer are related to the DEMO plasma parameters which are characterized by a very high temperature at the pedestal layer compared with that of ITER. In figure 2(c), the electron temperature profile is also shown in the SOL layer. Although knowledge of the density and temperature profiles in the SOL of ITER as well as in

DEMO is poor, based on edge transport codes (e.g. EDGE2D/Eirene) and different transverse transport coefficients, the electron temperature in the SOL of DEMO can be estimated in the range of 20 eV (see [46]). Several SOL profiles of T_e are used in the calculation of parametric instability in order to show the sensibility of the Fokker–Planck calculation in several edge conditions. We have
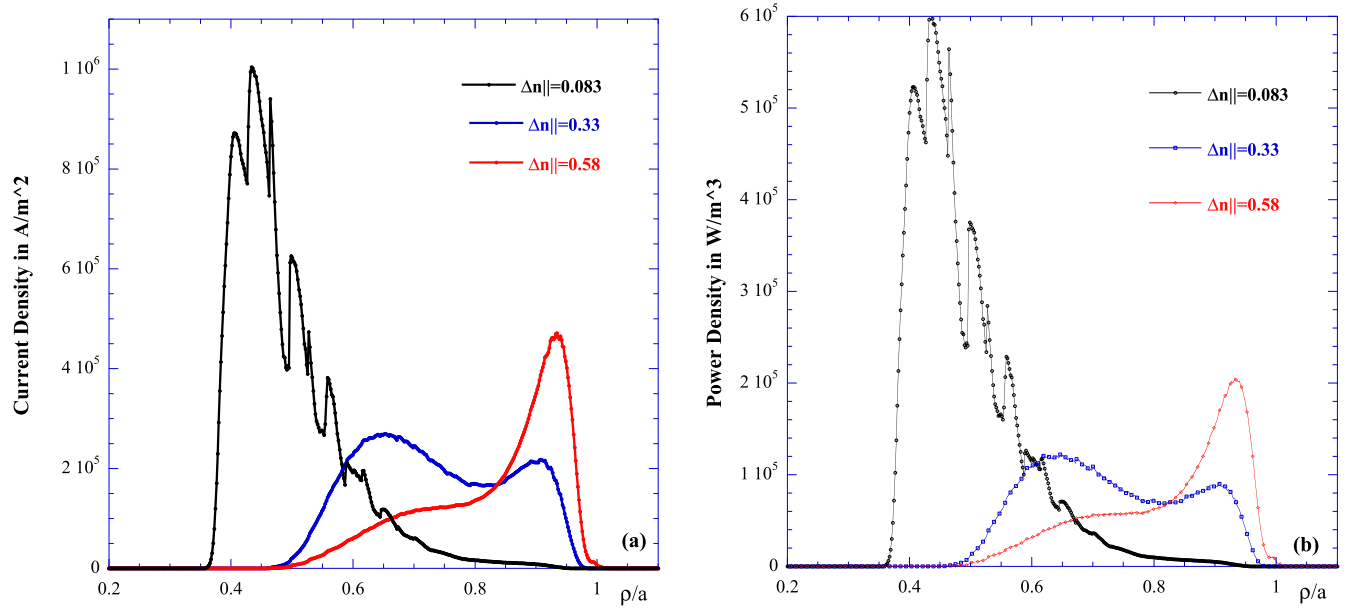
Figure 3. (a) j_{LH} profiles obtained respectively using the narrow (black curve), intermediate (blue curve), and broad (red curve) main lobe of antenna spectra of figure 1. Toroidal magnetic field: $B_T = 6.8$ T, plasma current: $I_P = 18$ MA, operating LH wave frequency: 5 GHz, absorbed RF power: 80 MW, antenna directivity: 60%. In the calculation it has been considered the 'peaked' DEMO scenario with kinetic profiles shown in figures 2(a) and (b) (blue curve). (b) Power deposition profile in W m^{-3} related to the same current density profile of figure 3(a).
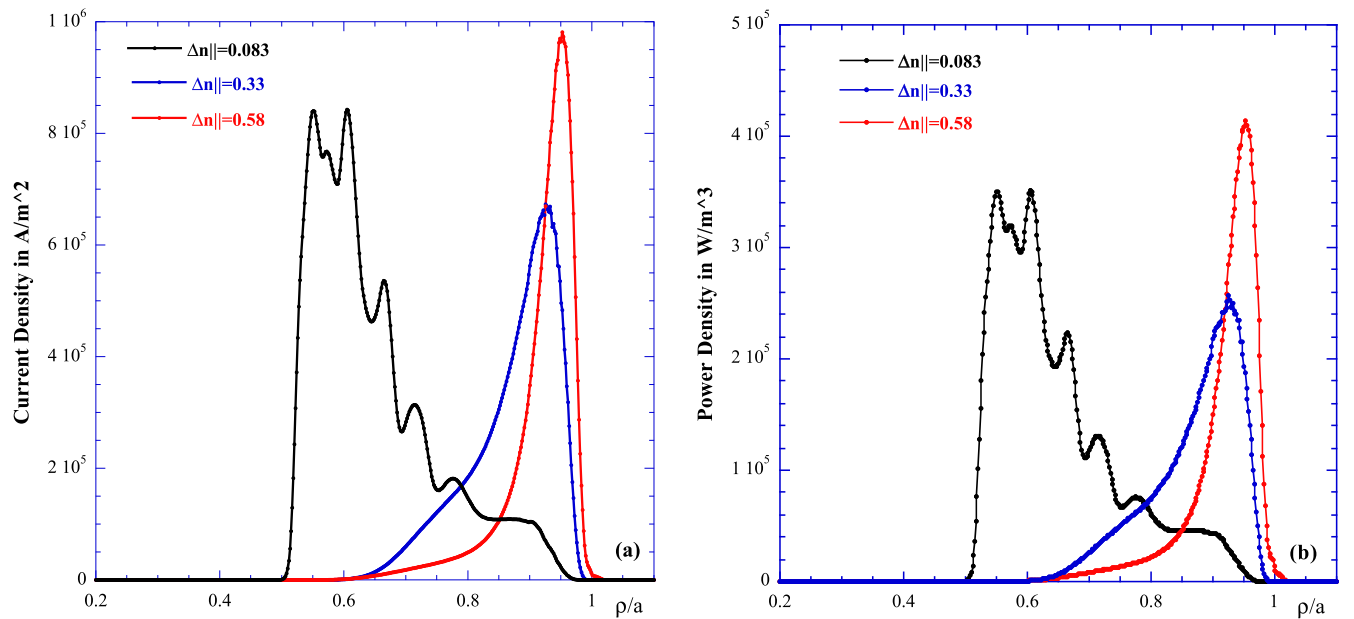

Figure 4. (a) j_{LH} profiles modelled, for the case of DEMO 'flat' scenario with kinetic profiles shown in figures 2(a) and (b) (red curve), using the antenna spectra of figure 1. (b) Power deposition profile in W m^{-3} related to the same current density profile of figure 4(a).

assumed that the density in the SOL behaves like $\exp[-\lambda^{-1}(x - x_{sep})]$, (where the e-folding length λ is ≈ 20 cm) because no effect on the propagation and PI activity was detected by varying the SOL density.

For the case of the peaked profiles of figure 2 (blue curve), the profiles of the current drive density j_{LH} are modelled by using antenna spectra with the three different spectral widths of figure 1. Figures 3(a) and (b) respectively show the current and power density profiles. They emphasize

the following feature: narrower antenna spectra produce j_{LH} profiles peaked at inner radii (at $r/a \approx 0.95$ for $\Delta n_{//} = 0.58$, at $r/a \approx 0.65$ for $\Delta n_{//} = 0.33$, and at $r/a \approx 0.45$ for $\Delta n_{//} = 0.083$).

For the case of a 'flat profile' (figures 2(a) and (b) (red curve)), a slightly more off-axis deposition is obtained as shown in figures 4(a) and (b), owing to higher T_e values (at half plasma radius: $T_e = 16$ keV compared to $T_e = 14$ keV for the peaked case). Only the narrower spectrum ($\Delta n_{//} = 0.083$) still drives
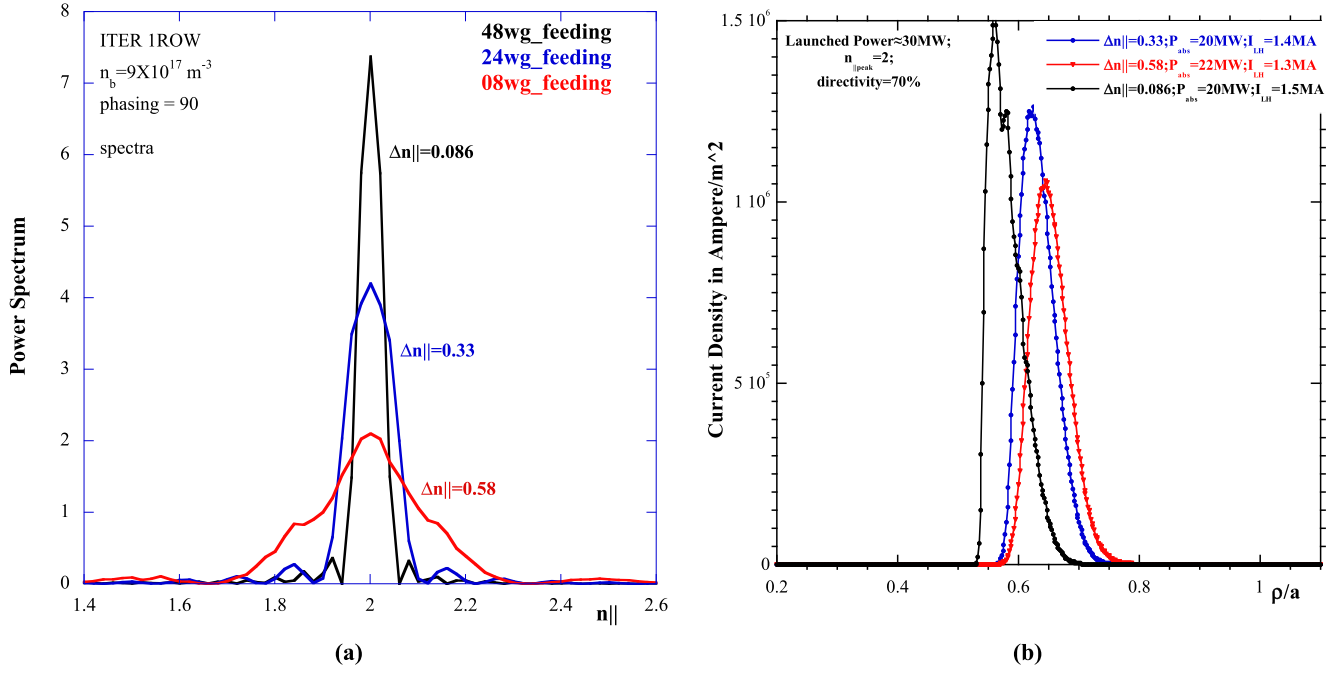
Figure 5. (a) Power spectra of the ITER antenna calculated with Grill-3D for a row made of a different number of waveguides. (b) j_{LH} profiles obtained in ITER plasma using previous spectra.

the current close to the middle radius. Note that for the case of DEMO flat (figure 2(a)), an analysis at a higher magnetic field (8.5 T) has been performed in [12]. Just to complete our analysis, we will show a case of ITER scenario 4 and compare it with DEMO results. In figure 5(a), the wave spectrum of the ITER antenna [42] as obtained by using our coupling code Grill-3D is shown. The narrow spectrum is essentially the nominal one, while the others have been obtained by considering a smaller number of waveguides per antenna row. The results are shown in figure 5(b) where the current driven as a function of the radius is plotted for the three spectra of figure 5(a). As it is possible to see the deposition layer does not change so much and is localized between $0.55 < r/a < 0.65$.

Figure 6 shows the j_{LH} profile obtained considering the whole antenna spectrum (a) and only that part of the spectrum which corresponds to the main lobe (b) of figure 1. This lobe is displayed in figure 7(a), juxtaposed to the highest lobe for negative parallel wavenumbers of figure 7(b). The latter is located at $n_{//0} = -3$ and produces a peak in the current density close to the separatrix. By using this whole spectrum, the total absorbed power ($\approx$80 MW) drives a net current ($\approx$3.8 MA) consistent with the result ($P_{abs} \approx 52$ MW and $I_{CD} \approx 3$ MA) obtained for the corresponding case shown on the same figure 6 (label b) where only the main lobe of spectrum of figure 1 and the antenna directivity ($dir = 60\%$) have been considered (here the co- and counter-current driven by the minor lobes have not been included).

It is interesting to note that the LHCD efficiency (defined as: $\eta_{LHCD} = R_0 \langle n_e \rangle I_{CD}/P_{CD}$) in these calculations results as: $\eta_{LHCD} = 0.3 \times 10^{20}$ A · W^{-1} · m^{-2}, a value in agreement with the most optimistic expectations [42].

The above results on LH penetration and QL absorption are favored mainly by the fact that the spectral width $\Delta n_{//}$ is
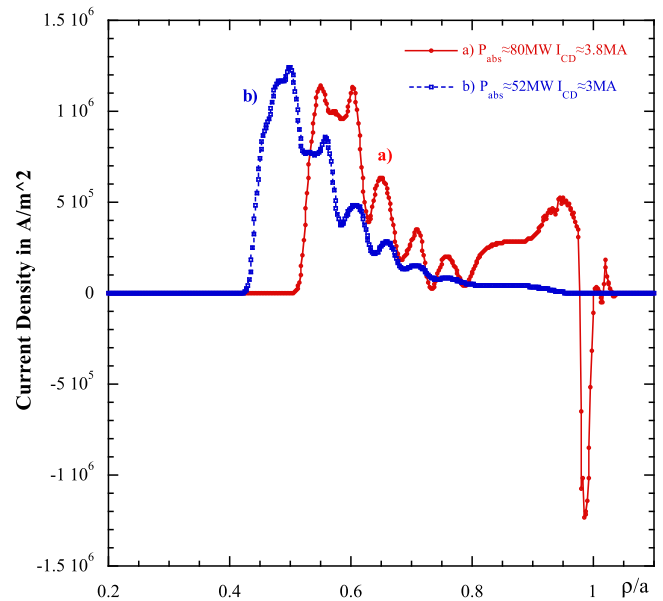

Figure 6. j_{LH} profiles obtained considering the whole antenna spectrum (a) displayed in figure 7, and the main lobe of the spectrum (b) as sketched in figure 1 ($\Delta n_{//} = 0.083$), and the plasma parameters related to DEMO flat case. Here, the large peak for negative $n_{//}$ ($n_{//} = -3$) produces a peak in the current density close to the separatrix. By using this whole spectrum, the total absorbed power ($\approx$80 MW) drives a net current ($\approx$3.8 MA). In the case where only the main lobe of spectrum is considered (label b) ($dir = 60\%$) a current of $\approx$3 MA is driven by 52 MW of absorbed power.

decreasing as the wave front moves inwards along the rays. This is due to the very low absorption of the central $n_{//0}$ component where the EDF is almost flat (plateau) while the main absorption of the spectrum takes place at the low and
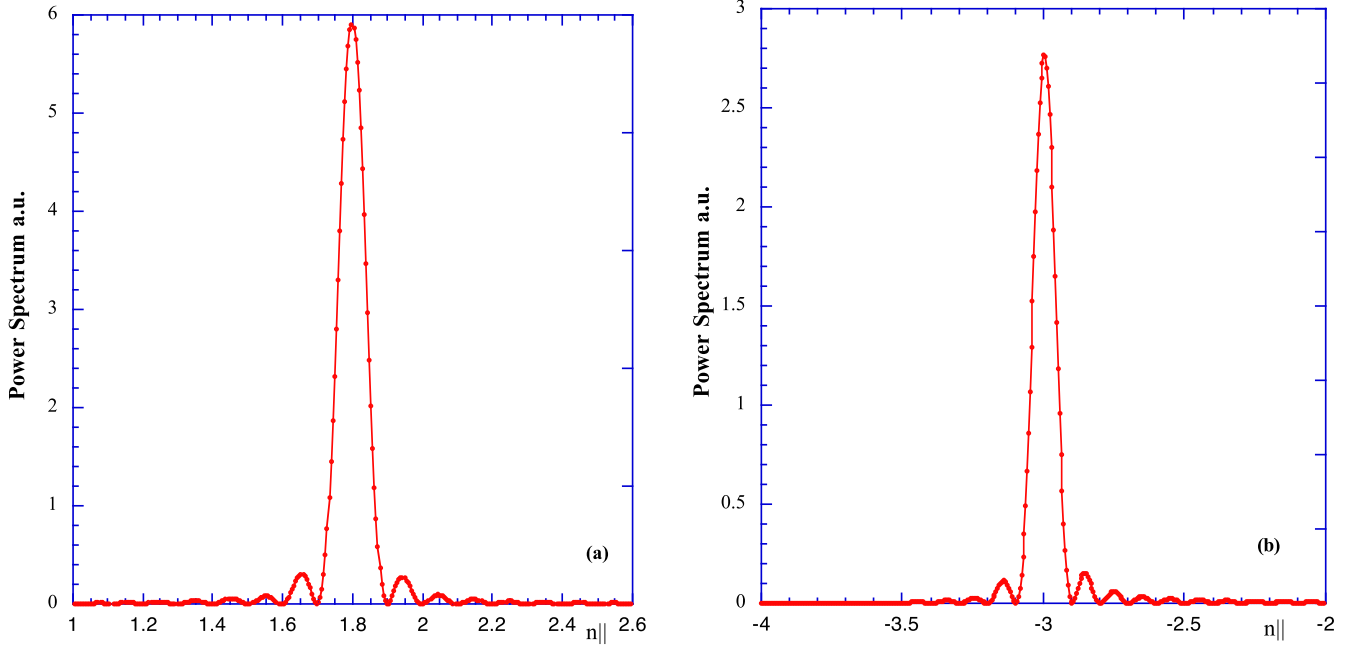
Figure 7. Whole antenna spectrum with $n_{//0} = 1.8$ when $n_{//} > 0$ (case a) and $n_{//0} = -3$ for $n_{//} < 0$ (case b), used for the current drive profiles of figure 6, and for the case of DEMO 'flat' profiles.

high side. In fact, we recall that the power absorption coefficient $k_\perp^{\text{Im}}(n_{//})$ is defined as

$$k_\perp^{\text{Im}}(n_{//}) \propto \left(\frac{df_e}{dv_{//}}\right)_{v_{//}=c/n_{//}} \propto \left(f_e \frac{C_{\text{coll}}}{D_{\text{QL}} + C_{\text{coll}}}\right) \quad (2)$$

where f_e is the EDF in the plateau region. D_{QL} and C_{coll} are the QL diffusion coefficient and the collisional operator respectively. Thus, absorption is small in the plateau centre around $n_{//0}$ where $D_{\text{QL}} \gg C_{\text{coll}}$, and much higher at the plateau sides $D_{\text{QL}} \approx C_{\text{coll}}$. In our numerical simulation, this feature is automatically present and well verified. Moreover, the delicate playing of spectral changes and absorption of the QL plateau regime is responsible for the minor oscillation of the LHCD radial profiles of figures 3 and 4.

Another test present in our modeling is the checking of QL limit validity. Indeed, a spectrum that is too narrow could be incompatible with the QL theory limit, since such a spectrum would significantly modify the electron orbits in the presence of excessively large RF power density (p_{RF}). Consequently, a trapping effect would occur, incompatible with the hypothesis of trajectory linearization that is at the basis of the QL model [19]. In the present analysis, QL theory validity can be investigated by considering the worst case corresponding to the narrow main lobe ($\Delta n_{//} = 0.083$) of figure 1. The phase velocity width is ($\approx 0.17c$) found to be much larger than the trapping velocity width ($\approx 0.002c$, for $p_{\text{RF}} \approx 30$ MW m^{-2}). The realistic values of the minimum and maximum phase velocities of the propagating wave spectrum, capable of altering the equilibrium EDF f_e, have been calculated near the absorption radial layer ($r/a \approx 0.5$), via ray-tracing and Fokker–Planck analyses, that properly describe wave propagation and absorption [22]. A wave electric field with intensity (0.2 kV cm^{-1}) markedly larger than that (0.05 kV cm^{-1})

expected to occur at this layer has been considered, with the aim of overestimating the above trapping velocity width, thus checking the QL theory validity with a larger margin.

A parasitic PI effect would not present a problem for LHCD in a reactor, thanks to the high temperature envisaged even at large radii [4, 29] (further support on this conclusion will be given further ahead in this paper). We have, however, considered the impact on the j_{LH} profile produced by the PI broadening of the launched antenna spectrum, in condition of two different T_e radial profiles of scrape-off layer (SOL), connecting the main plasma profile in two different ways (respectively, by exponential and exponential-square functions), which produce a marked difference (of around 35%) at radii close to the antenna. A radial gap (of about 25 cm) separates the antenna from the LCMS (Last Closed Magnetic Surface) layer where $T_e \approx 2$ keV. For the two considered profiles, the SOL-layers with relatively low T_e (≈ 20–40 eV) occur at slightly different radial distances from the antenna (respectively at: $d_{\text{ant}} \approx 3$ cm and $d_{\text{ant}} \approx 7$ cm for the exponential and exponential-square cases). This cold plasma region becomes unstable for PIs driven by ion-sound, evanescent, low frequency modes (~ 1 MHz) [25], with a more marked effect for the considered colder case. Consequently, some fraction (p_{PI}) of the RF power coupled by the antenna is redistributed over LH sideband waves ($p_{\text{PI}} \approx 1\%$ and $p_{\text{PI}} \approx 10\%$, respectively, for the exponential and the exponential-square profiles), resulting in a larger spectral broadening for the case of colder plasma edge (from $n_{//\text{cut-off}} \approx 3$ to $n_{//\text{cut-off}} \approx 5$). The broadening in frequency of the launched spectrum is quite small: $\leqslant 1$ MHz). Cases of larger extension of the mentioned cold layer ($\gtrsim 10$ cm) would produce a larger spectral broadening effect ($\gg 10\%$), which could not, however, be evaluated in the framework of the available
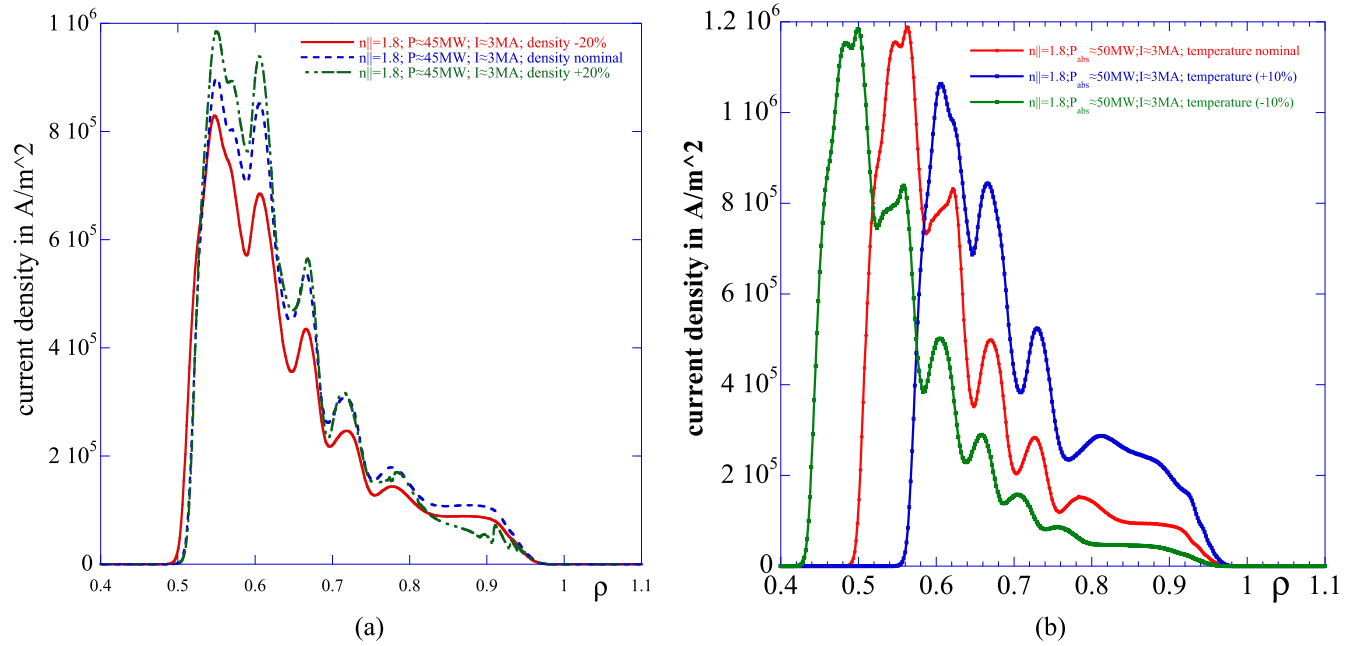
Figure 8. (a) Scan of plasma density. Effect of the radial density profile on the LH driven current: dotted (blue) curve: reference case of DEMO-flat. Green and red curves: same parameters but ±20% variation of plasma density. (b) Scan of electron tempertaure. Effect of the electron temperature profile on the LH driven current: red curve reference case of DEMO-flat profile; blue curve with same parameters but +10% higher plasma temperature; green curve with −10% lower plasma temperature. Note that the absorbed power in figure 8(a) is 45 MW for all cases while in figure 8(b) it is 50 MW. This explains the difference when using the nominal density and temperature profiles (blue curve of figure 8(a) and red curve of figure 8(b)).

modeling limit [25]. In any case, by including the strongest calculated effect of PI-spectral broadening, only minor changes to the j_{LH} profiles, driven current and absorbed power have been found, as we shall see later in this paper.

5. Further results and sensitivity analysis of the modeling

The above results have shown the possible penetration and absorption of LH waves from the periphery up to the middle minor radius of reactor plasma and thus LHCD can be tailored according the requests of the discharge needs. This is possible since high power density and narrow enough spectral width make the QL theory predict far less absorption at the plasma edge than in other cases (such as linear ELD). To better underline the nature of these results, we have used our code to predict how the CD current density profiles are sensitive to the variation of the plasma target or of the launched wave characteristics.

The DEMO 'flat' profile of figure 2 has been taken as a reference (a less favorable case, with 80 MW of coupled power and the narrow antenna spectrum of figure 1, centered at $n_{//0} = 1.8$). All parameters but those under scan have been kept fixed.

(i) Scan in plasma density

The effect of ±20% varying plasma density on the RF-driven current density radial profiles (j_{LH}) is shown in figure 8(a). No significant changes have been found in the absorbed

power (∼50 MW), in the driven current (∼3 MA), or the fraction of the coupled RF power that is redistributed over the PI sidebands: PI ∼ 1%.

(ii) Scan in electron temperature, T_e

A change of ±10% in temperature profile does not produce any significant changes in the total absorbed power (∼45 MW) and driven current (∼3 MA). The effect of a change in T_e (±10%) on the profiles j_{LH} can be seen in figure 8(b) where we have fixed the plasma density (flat profile) and all the other parameters by varying only the temperature profile (the nominal and ±10% of the nominal). As can be seen on the plot above, the effect causes a slight change in the peak of the current density profile, which moves to around ±10% of the radial position.

(iii) The role of PI

In order to estimate the T_e effect on the PI fraction, the exponential and the exponential/square cases of SOL T_e profiles have been compared. Markedly lower T_e (of about 35%) occurs within the PI unstable radial layer, which is consequently larger for the exponential/square case with respect to the exponential case. In the former case, the PI fraction is about 10% compared to about 1% for the latter case. By including the largest considered PI (∼10%), only minor changes to the driven current and absorbed power have been found. Additionally, j_{LH} profiles are not significantly altered. These results are summarized in figure 9, where the j_{LH} profile (for the DEMO flat case) are displayed without PI
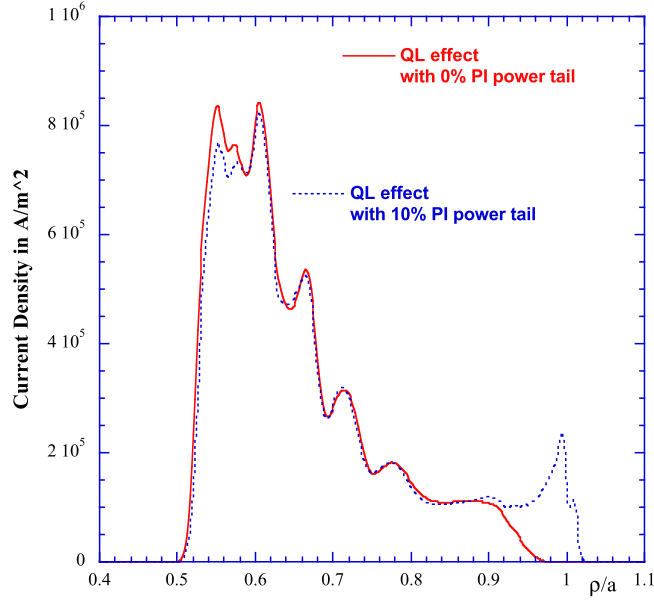
Figure 9. j_{LH} profiles with/without PI tail (10% of redistributed power).
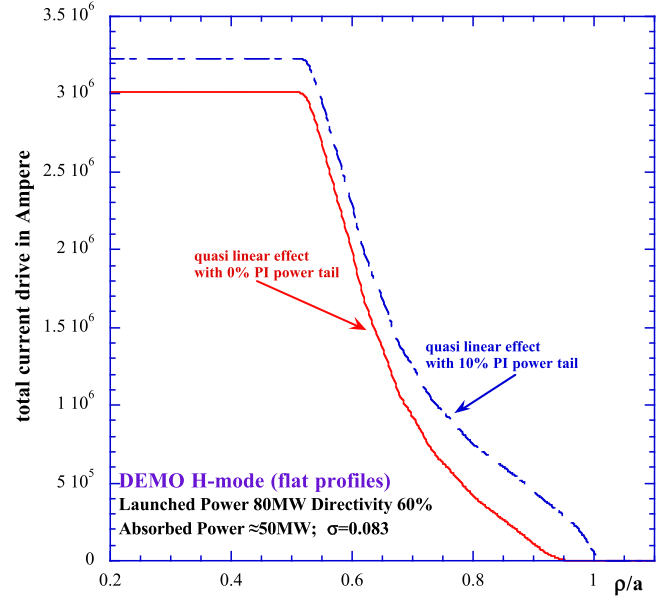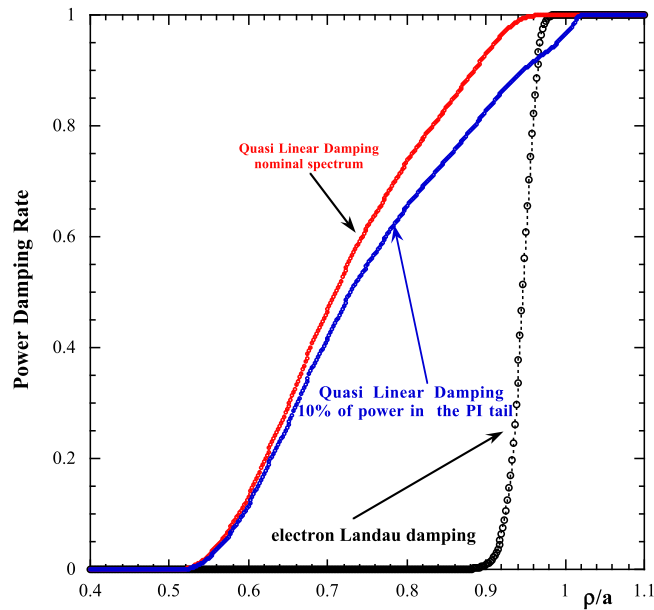

Figure 11. Total LH driven current.

Figure 10. Normalized power damping rate for cases: (i) linear only, (ii) QL, and (iii) QL + PI contribution.

Figure 12. Sensitivity of changes of the $n_{//}$ peak of the main lobe: $n_{//0} = 1.8$ (green), $n_{//0} = 1.9$ (blue), $n_{//0} = 2$ (black), $n_{//0} = 2.1$ (red), having fixed the width of the power spectrum to $\Delta n_{//} = 0.083$ (narrow case).

and with PI considered above PI ($\sim 10\%$). The relative normalized power ($P/P_0 = \exp\{-2\int_x^a k_\perp^{Im} dx\}$) is plotted in figure 10 where it is compared with that calculated retaining only the linear wave model (ELD absorption). Figure 11 also displays the total LH driven current for the above two cases with and without the PI spectral broadening contribution.

Importantly, this result is different from that relevant to LHCD experiments of JET, reported in [24, 25], where only little PI fractions dislocate the j_{LH} profile from the core to the outer radial half of the plasma, consequently enabling the transit from a multi-pass to a single-pass LHCD regime. This stronger effect of PI was indeed facilitated by the broader
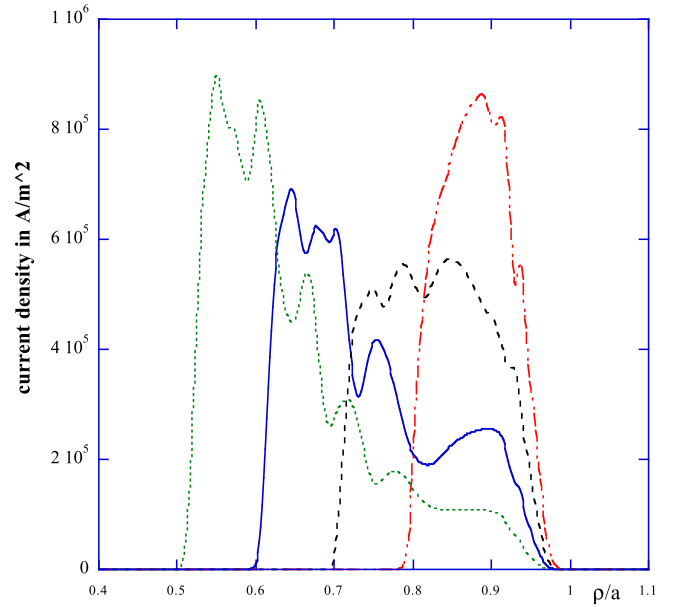
(initial) antenna spectrum utilized in the experiment than in the present modeling.

(iv) Scan in the position of the main lobe of the launched antenna power spectrum

The effect on the j_{LH} profile of the different position of the $n_{//}$ peak (in the range $n_{//} = 1.8 \div 2.1$) is shown in figure 12. The j_{LH} profiles move more and more at large radii when $n_{//}$ peak is increased, as expected. No significant change in the absorbed power, driven current and PI fraction occurs.
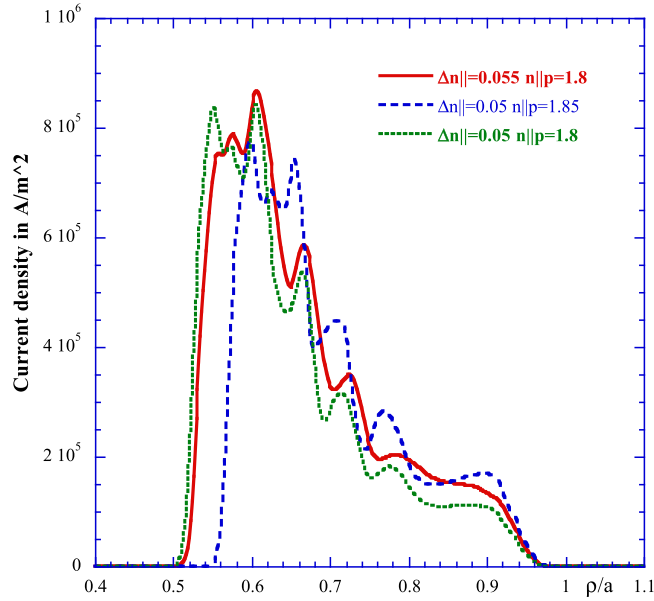
Figure 13. Sensitivity of changes of the width of the main lobe, for given $n_{//}$ peak ($n_{//0} = 1.8$), and $\Delta n_{//} = 0.05$ (green) and $\Delta n_{//} = 0.055$ (red) and for a given width ($\Delta n_{//} = 0.05$), and $n_{//0} = 1.8$ (red), and $n_{//0} = 1.85$ (blue).

(v) Scan in the width of the main lobe of the launched antenna power spectrum

In addition to examples contained in figures 3 and 4, the sensitivity of the changes of the $n_{//}$ spectral width has been verified for two given positions of the main lobe ($n_{//0} = 1.8$ and $n_{//0} = 1.85$), as summarized in figure 13. Again, no significant changes to the absorbed power, driven current and PI-spectral broadening are produced. In addition, we have performed further checks aimed at assessing the robustness of our results. Namely, we have changed the dimensions of the mesh and other parameters of the numerical computation. Consequently, no changes to the obtained results have been found.

6. Conclusive remarks

A major conceptual problem for a thermonuclear fusion reactor consists in the lack of an efficient method for driving with continuity currents in the outer radial half of a plasma column. Numerical simulation results shown here demonstrate that this problem could be solved by a suitably narrow power spectrum in the refractive index which enables LH waves to reach and interact with the hot plasma core of the reactor. The LHCD tool would thus guarantee for DEMO the desired goal of producing non-inductive current density at any desired layer located in the outer radial half of the plasma, while the remaining radial coverage should be performed by the already available current drive method based on ion beam power. The operating frequency of 5 GHz considered here for a possible LHCD tool for DEMO is high enough to minimize the possible damping on fusion born alpha particles [47, 48], and is in the range of the available high power sources [49]. The antenna should be designed for a coupling power of

about 80 MW, with spectra with an $n_{//}$ peak value of about 1.8, and width ranging between $\Delta n_{//} = 0.083$ and $\Delta n_{//} = 0.58$ by acting on the active waveguide phasing and feeding of the various modules composing the antenna. A similar choice should be considered for an LHCD experiment on ITER.

The circumstances have shown here that the quasilinear plasma-wave effect of strong microwave power coupled to high-temperature plasma via a sufficiently narrow spectrum in a parallel refractive index enables lower hybrid waves to drive current in the radial region of reactor plasma not sufficiently covered by other tools available so far, allows us to reconsider the steady-state regime of a thermonuclear reactor. The latter regime was indeed considered unviable owing precisely to the lack of a suitable current drive tool such as that which we have presented here. The LHCD method would also help to deal with the challenge that is, however, also inherent to the pulsed reactor regime. The lower hybrid current drive tool is now fully supported by the know-how necessary for its exploitation in the warm and dense plasma of a thermonuclear reactor.

References

[1] ITER Physics Basis Editors, ITER Physics Expert Group Chairs and Co-Chairs, and ITER Joint Central Team and Physics Integration Unit. ch1: Overview and summary 1999 *Nucl. Fusion* **39** 2137
[2] Wagner F *et al* 2010 On the heating mix of ITER *Plasma Phys. Control. Fusion* **52** 124044
[3] Kessel C E *et al* 2015 Physics basis for an advanced physics and advanced technology tokamak power plant configuration: ARIES-ACT1 *Fusion Sci. Technol.* **67** 75–106
[4] Zohm H *et al* 2013 On the physics guidelines for a tokamak DEMO *Nucl. Fusion* **53** 073019
[5] Giruzzi G *et al* 2015 Modelling of pulsed and steady-state DEMO scenarios *Nucl. Fusion* **55** 073002
[6] Orsitto F P *et al* 2016 Diagnostics and control for the steady state and pulsed tokamak DEMO *Nucl. Fusion* **56** 026009
[7] Freidberg J P 2007 *Plasma Physics and Fusion Energy* (New York: Cambridge University Press)
[8] Fisch N J 1987 Theory of current drive in plasmas *Rev. Mod. Phys.* **59** 175–234
[9] Irzak M A and Shcherbinin O N 1995 Theory of waveguide antennas for plasma heating and current drive *Nucl. Fusion* **35** 1341–56

[10] Bibet P *et al* 2005 ITER LHCD plans and design *21st IEEE/ NPS Symposium on Fusion Engineering SOFE 05 (26–29 September 2005, Knoxville, TN)* 1–4

[11] Andrews P L and Perkins F W 1983 Spectral broadening of lowerhybrid waves by timedependent density fluctuations *Phys. Fluids* **26** 2546–57

[12] Cardinali A *et al* 2017 Active current drive for economic viability for thermonuclear fusion reactors *Nat. Comm.* submitted

[13] Fisch N J 1978 Confining a tokamak plasma with rf-driven currents *Phys. Rev. Lett.* **41** 873–6

[14] Bernabei S *et al* 1982 Lower-hybrid current drive in the PLT tokamak *Phys. Rev. Lett.* **49** 1255–8

[15] Drummond W E and Pines D 1962 Nonlinear stability of plasma oscillation *Nucl. Fusion Supplement* **3** 1049

[16] Kennel C F and Engelmann F 1966 Velocity space diffusion from weak plasma turbulence in a magnetic field *Phys. Fluids* **9** 2377–88

[17] Karney C F F, Fisch N J and Jobes F C 1985 Comparison of the theory and the practice of lower-hybrid current drive *Phys. Rev. A* **32** 2554–6

[18] Bonoli P T and Englade R C 1986 Simulation model for lower hybrid current drive *Phys. Fluids* **29** 2937–50

[19] Santini F 1991 Nonresonant electron velocity diffusion by lower hybrid waves in tokamaks *Comments Plasma Phys. Control. Fusion* **14** 199–216

[20] Diamond P H, Itoh S I and Itoh K 2010 *Modern Plasma Physics: vol 1, Physical Kinetics of Turbulent Plasmas* (New York: Cambridge University Press)

[21] Brambilla M 1978 Electron landau damping of lower hybrid waves *Nucl. Fusion* **18** 493

[22] Brambilla M 1998 *Kinetic Theory of Plasma Waves: Homogeneous Plasmas* (Oxford: Oxford University Press)

[23] Brambilla M and Cardinali A 1982 Eikonal description of HF waves in toroidal plasmas *Plasma Phys.* **24** 1187

[24] Cesario R, Cardinali A, Castaldo C, Paoletti F and Mazon D 2004 Modeling of a lower-hybrid current drive by including spectral broadening induced by parametric instability in tokamak plasmas *Phys. Rev. Lett.* **92** 175002

[25] Cesario R *et al* 2006 Spectral broadening of lower hybrid waves produced by parametric instability in current drive experiments of tokamak plasmas *Nucl. Fusion* **46** 462

[26] Ding B J *et al* 2013 Experimental investigations of LHW-plasma coupling and current drive related to achieving h-mode plasmas in EAST *Nucl. Fusion* **53** 113027

[27] Ding B J *et al* 2015 Investigations of LHW-plasma coupling and current drive at high density related to h-mode experiments in EAST *Nucl. Fusion* **55** 093030

[28] Baek S G *et al* 2014 Characterization of the onset of ion cyclotron parametric decay instability of lower hybrid waves in a diverted tokamak *Phys. Plasmas* **21** 061511

[29] Cesario R *et al* 2010 Current drive at plasma densities required for thermonuclear reactors *Nat. Commun.* **1** 274–81

[30] Castaldo C *et al* 2016 Influence of collisions on parametric instabilities induced by lower hybrid waves in tokamak plasmas *Nucl. Fusion* **56** 016003

[31] Cesario R *et al* 2014 Spectral broadening of parametric instability in lower hybrid current drive at a high density *Nucl. Fusion* **54** 043002

[32] Garcia J *et al* 2008 Analysis of DEMO scenarios with the CRONOS suite of codes *Nucl. Fusion* **48** 075007

[33] Amicucci L *et al* 2016 Current drive for stability of thermonuclear plasma reactor *Plasma Phys. Control. Fusion* **58** 014042

[34] Cardinali A 2000 Quasilinear absorption of the lower hybrid wave in tokamak plasmas *Recent Research Developments in Plasmas* vol 1 (Transworld Research Network Magazine) p 185

[35] Crisanti F *et al* 2002 JET quasistationary internal-transport-barrier operation with active control of the pressure profile *Phys. Rev. Lett.* **88** 145004

[36] Mailloux J *et al* 2002 Progress in internal transport barrier plasmas with lower hybrid current drive and heating in JET (Joint European Torus) *Phys. Plasmas* **9** 2156–64

[37] Castaldo C *et al* 2002 Effect of low magnetic shear induced by lower hybrid current drive on high performance internal transport barriers in the Joint European Torus (JET) *Phys. Plasmas* **9** 3205–8

[38] Schneider M, Eriksson L-G, Imbeaux F and Artaud J-F 2009 Self-consistent simulations of the interaction between fusion-born alpha particles and lower hybrid waves in ITER *Nucl. Fusion* **49** 125005

[39] Poli F M, Kessel C E, Bonoli P T, Batchelor D B, Harvey R W and Snyder P B 2014 External heating and current drive source requirements towards steady-state operation in ITER *Nucl. Fusion* **54** 073007

[40] Ceccuzzi S *et al* 2013 Lower hybrid current drive for DEMO: physics assessment and technology maturity *Fusion Sci. Technol.* **64** 748–61

[41] Gormezano C, Briand P, Briffod G, Hoang G T, N'Guyen T K, Moreau D and Ray G 1985 Lower-hybrid plasma heating via a new launcher the multijunction grill *Nucl. Fusion* **25** 419

[42] Hoang G T *et al* 2009 A lower hybrid current drive system for ITER *Nucl. Fusion* **49** 075001

[43] Bonoli P T, Harvey R W, Barbato E, Imbeaux F, Peysson Y and Forest C B 2003 Lower hybrid current drive assessment for ITER - FEAT *ITPA Meeting Steady-State Operation* San Diego, CA (USA), General Atomics. https:// fusion.gat.com/conferences/itpa2003/steady_state/SSEP% 20pdf/12_Forest_LHCD.pdf

[44] Bonoli P T 2006 Benchmarking of lower hybrid current drive codes with application to ITER-relevant regimes *Proc. 21st IAEA Fusion Energy Conf.* Chengdu, China, IT/P1-2.

[45] Decker J *et al* 2011 Calculations of lower hybrid current drive in ITER *Nucl. Fusion* **51** 073025

[46] Rubino G, Ambrosino R, Calabrò G, Pericoli Ridolfini V and Viola B 2016 Comparative analysis of the SOL plasma in DEMO using EDGE2D/EIRENE and TECXY codes *22nd Int. Conf. on Plasma Surface Interactions in Controlled Fusion Devices* Rome, Italy, P3.48. (https://doi.org/ 10.1016/j.nme.2016.11.004)

[47] Barbato E and Santini F 1991 Quasi-linear absorption of lower hybrid waves by fusion generated alpha particles *Nucl. Fusion* **31** 673

[48] Barbato E and Saveliev A 2004 Absorption of lower hybrid wave power by α-particles in ITER-FEAT scenarios *Plasma Phys. Control. Fusion* **46** 1283–97

[49] Heating and Current Drive and ITER Physics Basis Editors ITER Physics Expert Group on Energetic Particles 1999 Ch 6: Plasma auxiliary heating and current drive *Nucl. Fusion* **39** 2495

[50] Ponti G *et al* 2014 The role of medium size facilities in the HPC ecosystem: the case of the new CRESCO4 cluster integrated in the ENEAGRID infrastructure *2014 Int. Conf. on High Performance Computing Simulation (HPCS)* 1030–3